Electronic Supplementary Material (ESI) for Journal of Materials Chemistry A.

Supporting Information

Hybrid Methanol and Water Co-solvent Electrolyte for Zinc Ion Batteries to Operate at Extremely Cold Temperatures

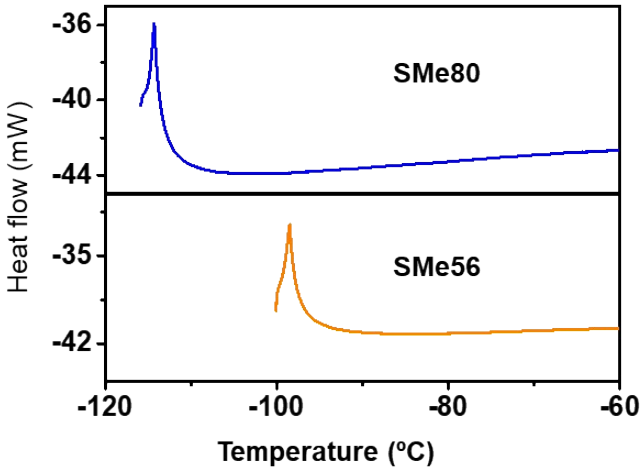

Figure S1. DSC curves of hybrid electrolytes

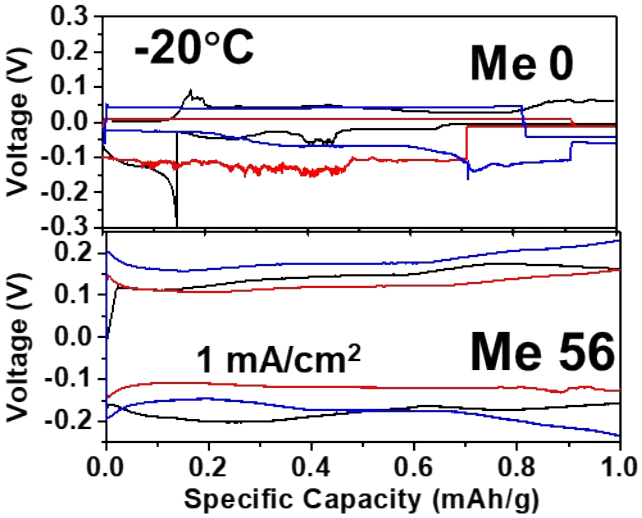

Figure S2. Voltage profiles for Zn//Zn symmetric batteries at -20 °C.

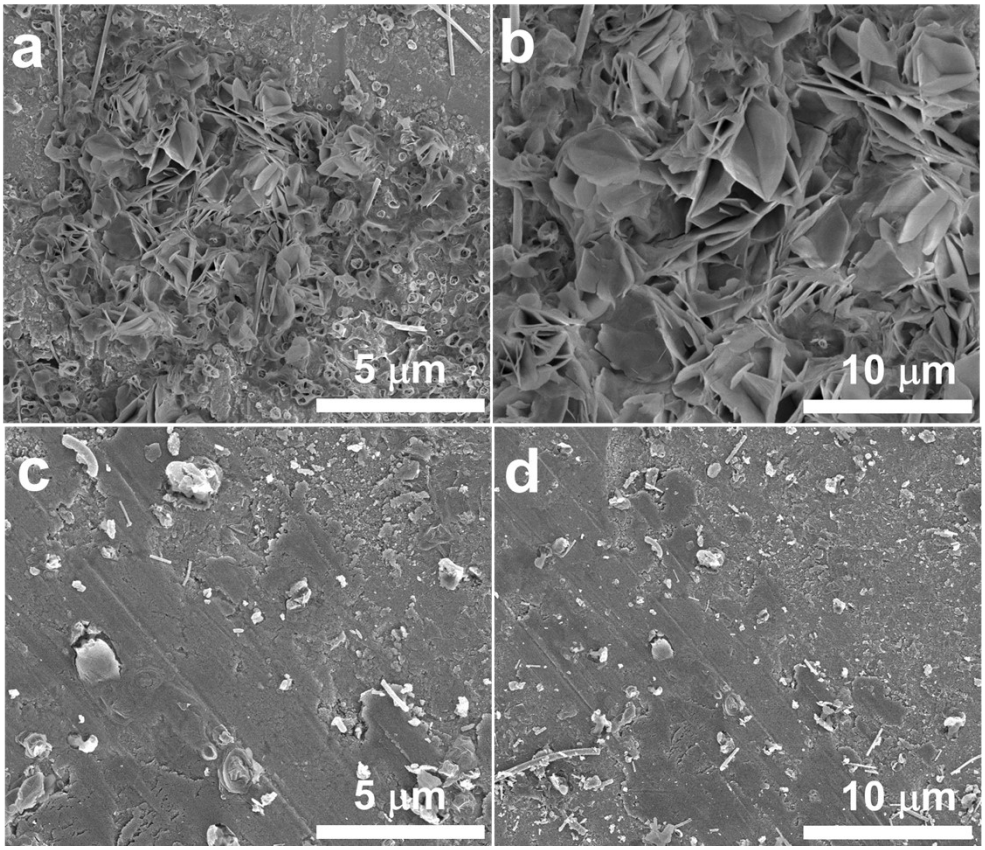

Figure S3. SEM images of Zn deposition with a capacity of 1 mAh/cm^2 after 50 cycles through Zn//Zn symmetric cells with (a, b) Me0 and (c, d) Me56 electrolyte.

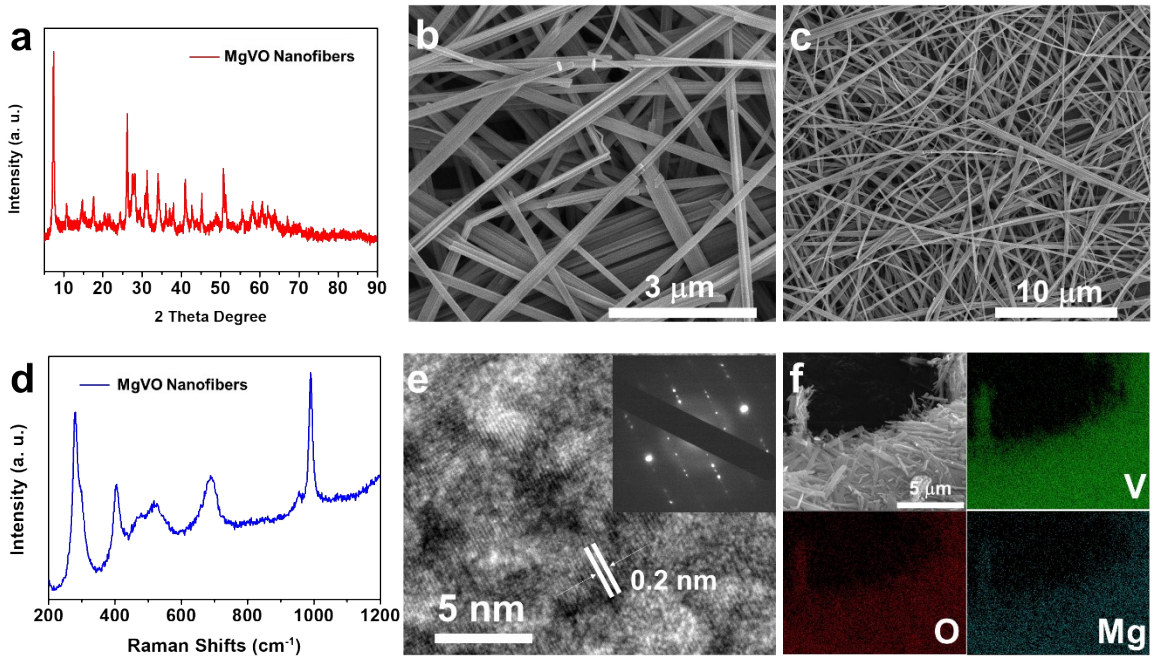

Figure S4. Material characterization of MgVO nanofibers. (a) XRD pattern, (b, c) SEM images, (d) Raman spectrum, (e) HRTEM images and corresponding SAED pattern, (f) EDS elemental mapping

The XRD pattern of $Mg_{0.3}V_2O_5{\cdot}1.0H_2O$ nanofibers exhibits several sharp diffraction peaks. The dominate peak at 7.3° corresponds to the (001) plane, showing a high preferred orientation along c-axis. The SEM images in Figure S3b and c confirm the nanobelt morphology with the width of 100-300 nm and length of 10-50 μm. The Raman spectrum data in Figure S3d show the peaks at 992.3, 690, 517.5, 404.3, 274 cm^{-1}. The peaks at 992.3, 690 and 517.5 cm^{-1} correspond to the stretching vibration of the V-O bonds. The characteristic stretching mode at 992.3 cm^{-1} reveals the layer-type crystal structure of synthesized $Mg_{0.3}V_2O_5{\cdot}1.0H_2O$. Figure S3e shows the high-resolution TEM images and SAED pattern of MgVO nanofibers. The spot pattern confirms the singlcrystal nature of the prepared MgVO nanofibers. EDS mapping in Figure 3f confirms the elemental composition. The vanadium, magnesium, and oxygen signals were overlapped uniformly across the entire sample.

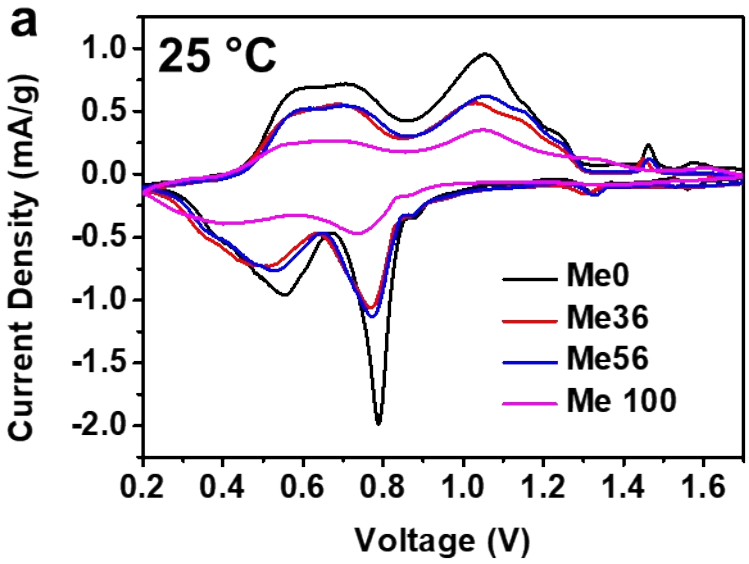

Figure S5. (a) CV curves of MgVO/Zn batteries with different hybrid electrolytes at 25 °C.

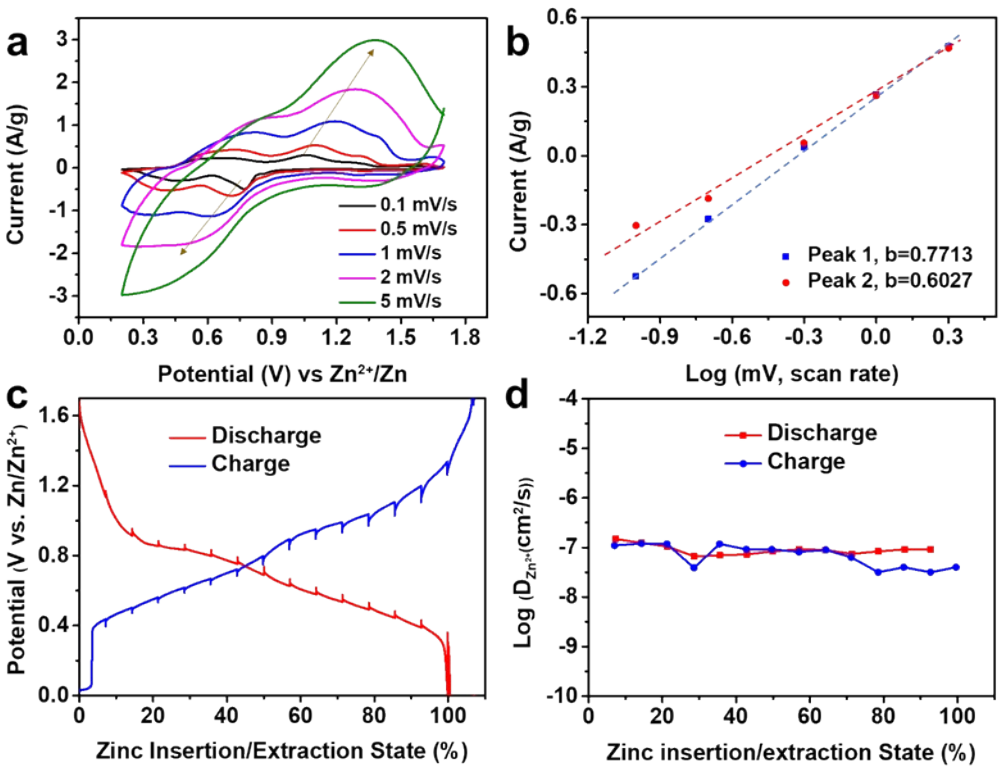

Figure S6. (a) CV curves at the scan rates of 0.1, 0.5, 1, 2 and 5 mV/s, (b) Randles-Sevcik plot of cathodic and anodic peaks, (c) GITT profiles of ZIBs with the Me56 electrolyte and (d) diffusion versus different Zn^{2+} insertion/extraction states

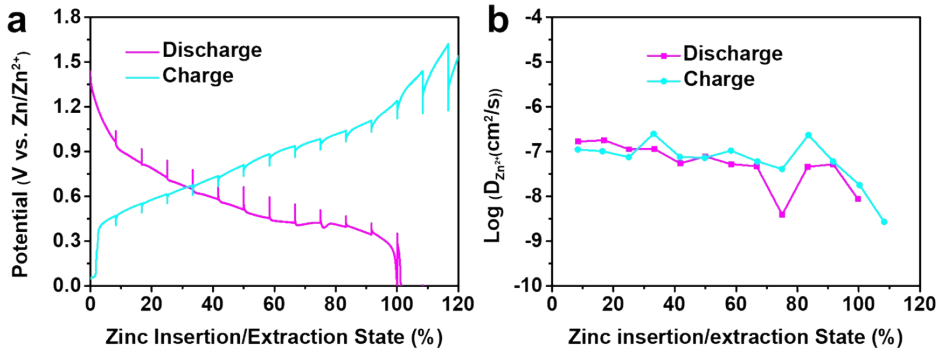

Figure S7. (a) GITT profiles of ZIBs with Me100 electrolyte, (b) diffusion versus different Zn^{2+} insertion/extraction states.

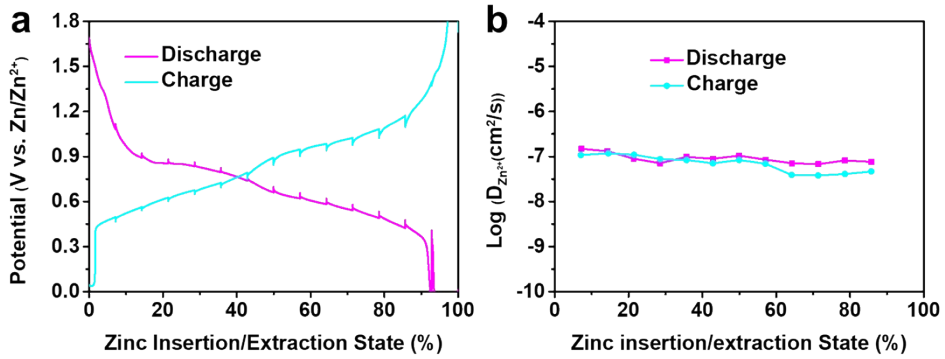

Figure S8. (a) GITT profiles of ZIBs with Me0 electrolyte, (b) diffusion versus different Zn^{2+} insertion/extraction states.

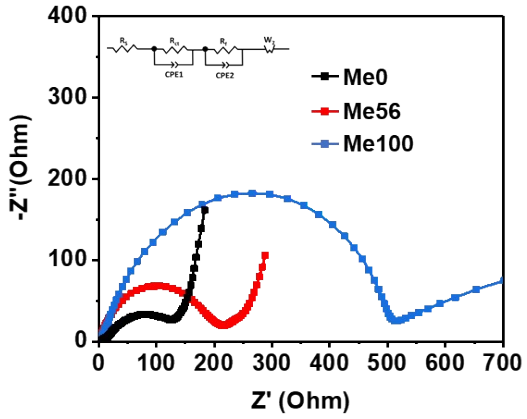

Figure S9. EIS spectra of the batteries at different electrolyte

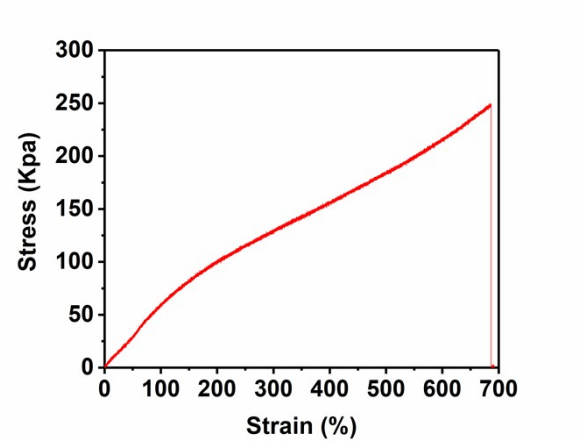

Figure S10. Stress-strain curves of CNF-PAM hydrogel electrolyte.

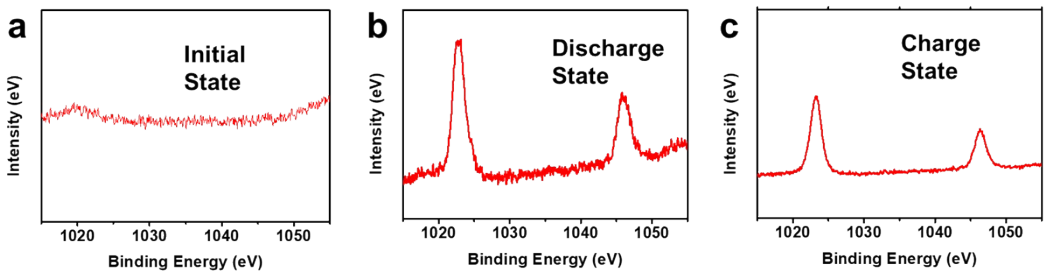

Figure S11. High-resolution XPS spectrum of Zn 2p at (a) initial, (b) discharge and (c) charge states.

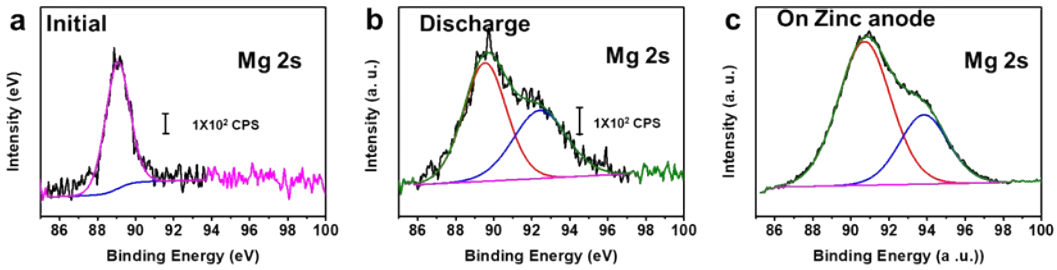

Figure S12. High-resolution XPS spectrum of Mg 2s at (a) initial, (b) 1st charge states and (c) Mg 2s on zinc anode electrode after 800 cycles.